Separation and Purification Technology 360 (2025) 130596

Contents lists available at ScienceDirect

Separation and Purification Technology

journal homepage: www.elsevier.com/locate/seppur

Enhancement of microplastics and nanoplastics removal via filtration method using surface-engineered palm kernel shell biochar

Muhammad Adli Hanif [a], Naimah Ibrahim [a,b,*], Nur Adlyna Hayazi [a], Farrah Aini Dahalan [a,b], Umi Fazara Md. Ali [c], Aishah Abdul Jalil [d,e], Achmad Syafiuddin [f]

[a] Faculty of Civil Engineering and Technology, Universiti Malaysia Perlis, 02600 Arau, Perlis, Malaysia
[b] Centre of Excellence for Water Research and Environmental Sustainability Growth (WAREG), Universiti Malaysia Perlis,02600 Arau, Perlis, Malaysia
[c] Faculty of Chemical Engineering and Technology, Universiti Malaysia Perlis, 02600 Arau, Perlis, Malaysia
[d] Faculty of Chemical and Energy Engineering, Universiti Teknologi Malaysia, UTM Johor Bahru, 81310 Skudai, Johor, Malaysia
[e] Centre of Hydrogen Energy, Institute of Future Energy, UTM, 81310 Johor Bahru, Johor, Malaysia
[f] Department of Public Health, Universitas Nahdlatul Ulama Surabaya, Surabaya 60237, Indonesia

ARTICLE INFO

Editor: V Tarabara

Keywords:
Plastic pollution
Microplastics
Nanoplastics
Pyrolysis
Biochar
CTAB
Filtration

ABSTRACT

Microplastics (MP) and nanoplastics (NP) are major aquatic contaminants, raising concerns due to their strong affinity for other toxic substances. Filtration is widely employed for MP and NP removal due to its simplicity, efficiency and variety of available filtration media. In this study, the removal efficiency of MP and NP was investigated using surface-engineered biochar of palm kernel shell (PKS) origin, modified with cetyltrimethylammonium bromide (CTAB). The modified biochar demonstrated performance superior to the unmodified biochar, achieving 95.71 % and 96.12 % polyethylene MP (2–4 μm) removal efficiency as measured by turbidity and gravimetric methods, respectively, at an optimal CTAB concentration of 1.5CMC. The optimized biochar (PKS-1.5CMC) also improved the removal efficiencies for a range of other MP and NP particles varying in size (159 nm–48 μm), shape (irregular, spherical, fibrous) and polymer type (polyethylene, polyamide). The modification with CTAB increased the biochar's surface positive charge and hydrophobicity, resulting in stronger electrostatic attraction and hydrophobic interactions with MP and NP particles, which are negatively charged and hydrophobic by nature. In terms of MP and NP properties, higher removal efficiencies were obtained for (i) larger MPs due to easier retention, (ii) NPs due to their tendency to agglomerate, resulting in larger particle size, (iii) irregularly shaped particles, because of their surface roughness, providing more attachment sites and (iv) polyethylene MPs and NPs, owing to their higher hydrophobicity and lower negative zeta potential. Significant formation of a cake layer observed on the upper surface of the filter media suggested that filtration, rather than adsorption, was the dominant mechanism for the removal of MP and NP by biochar.

1. Introduction

Microplastics (MP) and nanoplastics (NP) are plastic particles smaller than 5 mm and 1 μm, respectively, and are currently recognized as highly prevalent pollutants, especially in aquatic environments. These miniscule-sized pollutants originate either from the degradation of larger plastics or are specifically manufactured at these sizes [1,2]. In Malaysia, numerous studies have reported the presence of MP and NP particles across various sampling sites, with the highest magnitude of pollution recorded in a river on the east coast of Peninsular Malaysia, ranging from 22.8 to 300.8 MP and NP particles per m^3 [3]. In addition, personal care products, one of the largest contributors to anthropogenic MP and NP pollution, are estimated to release approximately 0.2 trillion particles into aquatic ecosystems annually [4]. The presence of MP and NP in aquatic ecosystems is a major concern, as they have a high affinity for various pollutants and can be ingested by marine organisms, leading to bioaccumulation and transfer through the food chain to higher trophic levels [5,6]. Given the challenges of significantly reducing plastic usage in the near future and the public lack of awareness regarding MP and NP pollution [7], the most effective current strategy is to improve the performance of available MP and NP removal methods.

Various methods have been employed to mitigate MP and NP

* Corresponding author at: Faculty of Civil Engineering and Technology, Universiti Malaysia Perlis, 02600 Arau, Perlis, Malaysia.
E-mail address: naimah@unimap.edu.my (N. Ibrahim).

https://doi.org/10.1016/j.seppur.2024.130596
Received 8 September 2024; Received in revised form 13 November 2024; Accepted 17 November 2024
Available online 26 November 2024

pollution in aquatic environments, including filtration, coagulation, flocculation and sedimentation, adsorption, electrocoagulation and photocatalytic degradation. Filtration is among the most commonly used methods due to its simplicity, high efficiency and the variety of available filters [8]. In this process, MP and NP particles are separated from a solution by being retained by the filter, allowing cleaner water to pass through as effluent [9]. Filters used in filtration can be classified into two main types: (i) membrane or (ii) filter media. In membrane-based filtration, MP and NP particles can be captured through two mechanisms: (i) cross-flow filtration, where MP and NP-containing solution flows in tangent across the filter surface, and (ii) dead-end filtration, where the solution flows in perpendicular through the filter [10]. Due to the structure of the filter media, filter-media-based filtration may solely operate through the latter mechanism.

Membrane-based filtration may be further classified based on the size of uniform pores: (i) microfiltration (0.08–2 μm), (ii) ultrafiltration (5–20 nm) and nanofiltration (~2 nm) [9]. Various membranes have been employed in MP and NP removal studies, including polyvinylidene fluoride [11–13], polyethersulfone [14], polyurethane [15], polycarbonate, cellulose acetate and polytetrafluoroethylene [16], etc. with removal efficiencies ranging from 82 to 100 %. However, since the membranes are synthesized from plastic polymers, prolonged use may result in membrane abrasion, leading to secondary plastic pollution. In contrast, non-plastic filter-media-based filtrations do not contribute to plastic pollution, although they often show weaker and more inconsistent performance than membrane-based systems. Porous materials such as sand [17–19], zeolites and molecular sieves [20], activated carbon [21,22], biochar [23,24], and limestone [25] have been investigated for MP and NP removal.

Biochar is highly appealing for the removal of MP and NP in aqueous solution mainly due to its sustainable production from the pyrolysis of biomass, often derived from wastes or byproducts of other applications. This not only reduces waste and mitigates environmental issues but also generates high-value products. Biochar has been employed for the removal of MP and NP through various methods e.g. coprecipitation, batch study, column-based removal etc. [26,27]. Among these, continuous flow column-based removal is particularly practical, as it is more realistic for large-scale continuous water treatment systems. Various waste materials, such as jujube waste, lignin, cellulose, woodchips, corn straw, hardwood, Scots pine barks, spruce bark, rice husk, and banana peel have been utilized as filter media and were reported to effectively remove MP particles through column-based filtration [23,24,28–31]. Due to the biochar's rough surface, porous structure and tuneable surface properties (zeta potential, hydrophobicity), these studies reported that the biochar-based filtration system remove MP and NP particles through mechanisms like entanglement with biochar particles, pore entrapment, electrostatic attraction and hydrophobic interactions. Ahmad et al. [23] achieved the highest reported removal efficiency with over 99 % of 1–10 μm polyethylene and nylon particles removed using jujube waste-based biochar. However, existing studies on biochar-based filtration have been primarily focused on plastic particles bigger than or equal to 1 μm in size, leaving the transport behaviour of smaller NP particles through biochar filter media largely unexplored. Moreover, several studies have integrated biochar with sand filters in filtration columns, making it challenging to attribute the removal efficiency solely to biochar. Additionally, most research has utilized plastic particles of uniform shape, which does not fully represent the complexity of MP and NP found in the environment [32].

Most MP and NP particles, as well as biochar, are negatively charged and hydrophobic. As a result, these materials can either interact through hydrophobic forces or repel each other electrostatically. To improve removal efficiency, biochar can be modified to carry a net positive charge and increase its hydrophobicity, thereby enhancing interactions via electrostatic attraction and elevated hydrophobic forces. Shen et al. [20] demonstrated that modifying zeolite and molecular sieves with hexadecyl pyridinium bromide (HDPB), a cationic surfactant, significantly improved MP removal compared to unmodified aluminosilicates filter media. However, HDPB is toxic and must be properly controlled to avoid leaching, which could severely contaminate the effluent. An alternative cationic surfactant, cetyltrimethylammonium bromide (CTAB), is non-toxic and has been used to alter the properties of various materials for enhanced removal of negatively charged pollutants such as hexavalent chromium [33], dyes [34–37], nitrates [38,39] etc. In the context of MP and NP removal, CTAB has been utilized to modify magnetic biochar for polystyrene-based MP and NP removal in batch studies by Shi et al. [40], Xing et al. [41] and Parashar & Hait [28], all of which achieved removal efficiencies between 90–99 %. Parashar & Hait [28] also studied MP removal in a fixed-bed column by integrating CTAB-modified magnetic biochar with a sand filter, achieving more than 97 % removal under optimal conditions. These studies concluded that CTAB enhances biochar's properties, leading to improved removal performance. However, as noted earlier, they have typically focused their work on single types of MP and NP polymers, shapes and sizes, which does not account for the diversity in the morphologies and characteristics of plastic pollutants present in real environmental conditions. Additionally, the use of magnetic biochar raises concerns about potential iron leaching, which could lead to secondary pollution [42]. These studies also did not optimize the CTAB concentration for the biochar modification, which is crucial to achieving maximum removal efficiency without excessive use of CTAB.

This study introduces a unique and effective approach for studying the removal of MP and NP across a range of particle sizes, shapes, and polymer types by employing CTAB-modified biochar derived from palm kernel shell, a widely available agricultural waste in Malaysia. To our knowledge, this is among the first studies to employ NP particles in a column-based filtration setup with biochar, offering unique insights into biochar's capacity to filter and adsorb extremely small plastic particles under dynamic conditions. Additionally, unlike previous research, which primarily involves magnetized biochar, the use of CTAB modification alone eliminates potential secondary pollution risks, while enhancing adsorption properties suitable for non-magnetic, eco-friendly applications. By optimizing the CTAB concentration, we have systematically improved the filtration performance, demonstrating practical applicability for sustained and effective MP and NP removal in continuous-flow systems.

2. Experimental

2.1. Preparation of biochar and surface-engineered biochar

The biochar was synthesized from palm kernel shells (PKS) collected from a local oil palm mill. PKS was thoroughly washed using distilled water, followed by oven drying at 110 °C to completely remove the moisture. The dried PKS was placed in a closed crucible and fully covered with aluminium foil to limit the exposure to oxygen. The sample was converted into biochar via slow pyrolysis using a muffle furnace in a limited oxygen environment at 600 °C at a heating rate of 5 °C/min for 4 h. The muffle furnace was equipped with a suction fan, which allows the elimination of surrounding gases and gases that formed during the pyrolysis process. The PKS-biochar obtained was then milled and sieved into a size range between 0.6 and 1.18 mm, selected based on our previous optimization study [43]. The milled biochar was then washed with distilled water to remove the remaining powdered particles attached to the biochar. The cleaned samples were oven-dried at 110 °C, labelled as PKS-Blank, and properly kept in a desiccator prior to usage. The surface-engineered biochar was prepared by introducing cetyltrimethylammonium bromide (CTAB) onto the PKS-biochar surface. Based on the value of CTAB critical micelle concentration (CMC = 0.335 g/L), three different concentrations of CTAB solution (1CMC, 1.5CMC, 2CMC) were prepared. The PKS-biochar was added into the CTAB solution at a ratio of 1:4 (w:v) and magnetically stirred overnight. The mixture was filtered using filter paper to retain CTAB-modified biochar,

followed by oven-drying at 65 °C for 4 h. The samples were then properly kept in a desiccator prior to their use. These CTAB-modified biochar samples were labelled as PKS-X, where X represents the concentration of CTAB.

2.2. Preparation of MP and NP samples

The performance of the surface-engineered biochar was examined using four different MPs of different polymer types, sizes, shapes and colours, as follows: (i) PE40-48 (polyethylene, 40–48 μm, irregular, blue; Sigma Aldrich), (i) PE2-4 (polyethylene, 2–4 μm, irregular, red; Sigma Aldrich), (iii) PA6-9 (polyamide, 6–9 μm, spherical, white; SH Energy & Chemical), and (iv) PAFibre (polyamide, < 5 mm, fibrous, green; obtained locally). The PE40-48 and PE2-4 samples were originally white but were stained blue and red, respectively, with coloured dyes for differentiation purposes. PAFibre, originally larger in size, was cut manually using scissors to achieve the desired MP size. The NP used in this study was prepared by wet milling larger MP particles (polyethylene, 125 μm, irregular, white; Sigma Aldrich). The wet milling process involved mixing MP with ethanol (99.9 %, HmBG) at a 2:1 (w/v) ratio, placing the mixture in a milling bowl and adding milling balls at a weight ratio of 10:1 relative to the dry MP mass. The sample was milled at 400 rpm for 24 cycles (each cycle comprising 5 min of milling followed by a 5-minute pause). The resulting particles were then analysed with a particle size analyser and labelled as PENano (polyethylene, 159 – 756 nm, irregular, grey; obtained via milling). Additionally, this study utilised a mixture of all five MP and NP samples in equal concentrations, referred to as MIX. The MP solution was prepared by mixing 0.05 g of MP and NP with a solution of distilled water and ethanol in a volumetric ratio of 9:1. The ethanol facilitates the reduction of surface tension and minimizes the agglomeration of MP and NP particles in the solution [44,45]. The pH of the solution was adjusted to 7 using hydrochloric acid or sodium hydroxide solution, and particle dispersion was further enhanced by magnetic stirring for 30 min before the removal study.

2.3. Characterization of samples

The physicochemical properties of the biochar, surface-engineered biochar, and MP and NP samples were characterized to evaluate their influence on the removal process. The surface chemistry of biochar and surface-engineered biochar was examined to determine whether CTAB modification of the biochar was successful. Functional group identification was conducted using Fourier transform infrared spectroscopy (FTIR) via Perkin Elmer Frontier FTIR in attenuated total reflection (ATR) mode. The spectra obtained between the wavelength range of 4000–600 cm^{-1} were compared with an FTIR database and relevant literature to verify the surface functional groups on the samples. The surface morphology of all samples was characterized by a field emission scanning electron microscopy (FESEM) using Zeiss Leo 1525 at a magnification between 100x and 30000x, depending on the sample size. Morphological properties from the micrographs were further analysed using ImageJ software.

To understand the possible interaction between the biochar and MP and NP particles, the hydrophobicity/hydrophilicity and zeta potential of all samples were measured. Hydrophobicity was determined using sessile droplet angle measurement based on the methods reported by Kumarasiri et al. [46]. A 3.5 μL of distilled water droplet was placed on the sample surface, and its image was captured using a digital microscope. The contact angle (θ) of the water droplet was measured using ImageJ software with contact angle plugins, and the average contact angle at three different points was recorded. Samples were classified as hydrophilic for θ smaller than 90°, hydrophobic for θ between 90° – 150° and superhydrophobic for θ larger than 150° [47]. The zeta potential of all samples was measured using a Malvern zetasizer Nano ZS. A 100 mg/L of each sample was dispersed in an aqueous solution, and the zeta potential was measured only at pH 7, with results reported in electron volts (eV).

2.4. MP and NP removal study

The MP and NP removal study was conducted via a continuous-flow dead-end filtration system in a column-based setup, as shown in Fig. 1. Biochar or surface-engineered biochar was packed into the middle section of a glass filtration column (l = 25 cm, d = 20 mm) with a bed height of 10 cm. The filter media was supported by glass beads on both sides to enhance water flow. The packing of the filter media was accomplished through an elution method, where distilled water was passed through the column to remove air voids. This process was repeated until a constant bed height was achieved. Based on the filter media size, the packing in the column resulted in a bed porosity (ε) of 0.400 and a tortuosity (τ) of 1.458. A very thin layer of wool was placed between the biochar bed and the lower glass bead layer to prevent the sudden movement of biochar particles into the effluent stream. The MP and NP solution was introduced into the column at a flow rate of 7 ml/min under gravitational assistance and facilitated by a peristaltic pump. The filtration process was conducted continuously for 2 h, and the effluent samples were collected every 5 min in glass bottles for subsequent analysis.

Based on the literature, MP particles larger than 20 μm have been efficiently removed through filtration [18][48]. To investigate the effectiveness of filtering smaller MP particles, this study employed PE2-4, which is significantly smaller than 20 μm. PE2-4 was also chosen due to its irregular shape, which is the most commonly reported MP shape found in the aqueous environments. Once the optimal CTAB concentration for surface-engineered biochar is determined, this biochar will be utilized for filtration of other MP and NP samples. The biochar's performance in MP removal will be evaluated through turbidity and gravimetric methods. Turbidity was selected as it has been reported to be more sensitive than the absorbance method [49]. Prior to the study, individual solutions of known MP and NP concentrations were prepared, and their turbidity was measured using a turbidimeter [50]. The turbidity data for each MP and NP solution were plotted in a calibration graph, each demonstrating a reliable coefficient of determination ($R^2 > 0.99$). The calibration equations for PE40-48, PE2-4, PA6-9, PAFibre, PENano and MIX solutions are summarized in Table 1 corresponding to Eqs. (1)–(6), respectively. During the experiment, effluent samples were

Fig. 1. Experimental setup of MP and NP removal study.

Table 1
Calibration equations and R^2 values for turbidity measurement of the different MP and NP samples.

Sample	Equation	R^2	Equation no.
PE40-48	y = 409.504x – 0.138	0.9983	(1)
PE2-4	y = 735.754x + 0.138	0.9998	(2)
PA6-9	y = 247.136x + 0.062	0.9996	(3)
PAFibre	y = 131.914x + 0.085	0.9992	(4)
PENano	y = 832.993x + 0.151	0.9996	(5)
MIX	y = 242.719x + 0.604	0.9998	(6)

collected every 5 min, and the MP and NP concentrations in both influents and effluents were estimated using these turbidity calibration lines. Turbidity removal (%), representing the MP removal efficiency throughout the experiment, was calculated using Eq. (1) as follows:

$$\text{Turbidity removal}\,(\%) = \frac{\text{Initial turbidity}\,(\text{NTU}) - \text{Turbidity at time t}\,(\text{NTU})}{\text{Initial turbidity}\,(\text{NTU})} \times 100\,\% \quad (1)$$

where initial turbidity refers to the turbidity of the influent solution due to the presence of MP particles before filtration, and turbidity at time t refers to the turbidity of effluent at each collection time interval, indicating the presence of remaining MP particles that have passed through the filter media. This comparison allows for calculating the removal efficiency of MP particles by the biochar filter over time.

In the gravimetric method, the collected effluents were filtered using appropriate filter papers depending on the size of MP and NP to ensure complete filtration. The filter papers used were (i) Smith 102 Qualitative (pore size = 8 – 11 μm), (ii) Whatman glass microfiber filter (pore size = 1 μm), and (iii) Nice nylon filter membrane (pore size = 0.22 μm). The mass difference before and after the filtration process was calculated and defined as the amount of MP and NP retained in the effluent, representing the MP and NP removal efficiency. The gravimetric removal (%) was calculated using Eq. (2), where initial mass refers to the initial MP and NP mass in the influent before filtration, and the final MP and NP mass refers to the MP and NP particles retained in the effluent.

$$\text{Gravimetric removal}\,(\%) = \frac{\text{Initial MP and NP mass}\,(\text{g}) - \text{Final MP and NP mass}\,(\text{g})}{\text{Initial MP and NP mass}\,(\text{g})} \times 100\,\% \quad (2)$$

Additionally, as the glass filtration column used in this study is transparent while the MP and NP particles are coloured, the maximum bed depth reached by the particles from the top was visually observed by the naked eye. The visual assessment provided supporting evidence on the transport behaviour of the particles through the biochar media.

2.5. Quality assurance and quality control

Quality assurance and quality control (QA/QC) are essential in MP and NP studies as samples are highly susceptible to cross-contamination from surrounding plastic particles, which could lead to inaccuracies, such as overestimation or underestimation of the results. Various QA/QC measures were employed in this study to ensure data reliability. All experiments were conducted using glass, metal or aluminium instruments and equipment to prevent potential plastic degradation. To further avoid contamination, the instruments were thoroughly washed and rinsed with distilled water and covered with aluminium foil when not in use, especially to prevent airborne plastic particles from contaminating the samples. Although ultrapure water is ideal and highly recommended for use in MP and NP studies, we had to use distilled water due to the lack of an ultrapure water production system in our lab. As distilled water may contain some impurities, it was pre-filtered with a filter membrane before use. Similarly, other chemicals, e.g., ethanol, were also pre-filtered before application. The MP and NP removal process was conducted in a makeshift container fully covered with aluminium foil, which is only accessible to the analyst's hands to limit exposure to potential contaminants. The cleanliness of the container and surrounding work area was maintained by regularly cleaning the workbench surface with pre-filtered ethanol. Additionally, analysts wore pure cotton lab coats and latex gloves during the experiments to prevent the introduction of plastic particles into the samples. A negative control was employed in this study by running blank samples to assess background contamination. These results were used to adjust MP and NP concentrations obtained from turbidity and gravimetric measurements. The experiments were conducted in triplicates, and the reported results reflected the average concentration obtained from these three trials. Error bars were omitted from data presentations if the variations between the experimental runs were minimal or negligible.

3. Results and discussion

3.1. Characterization of samples

The physicochemical properties of unmodified PKS biochar, surface-engineered biochar, and all MP and NP samples employed were analysed to determine the potential influence on MP and NP removal performance. FESEM micrographs and FTIR spectra of all biochar samples are presented in Fig. 2, while FESEM micrographs for MP and NP samples are provided in Fig. 3. Since the samples varied significantly in size, different FESEM magnifications were used for each MP and NP sample to capture relevant morphological details. The zeta potential and the water droplet contact angle measured to determine hydrophobicity are summarized in Table 2.

The FESEM micrographs in Fig. 2(a) show that PKS-Blank possesses a slightly rough surface with the presence of macropores ranging from 760 to 2192 nm. In contrast, the surface-engineered biochar, PKS-1CMC, PKS-1.5CMC and PKS-2CMC, shown in Fig. 2(b), (c) and (d), respectively, demonstrate increasingly uniform pores, smoother surfaces and a reduced presence of fine biochar particles with an increment in CTAB concentration. This observation corroborates the findings by Wang et al. [37] and Mondal & Majumder [51], who also reported surface smoothening after introducing CTAB to pine nut shell biochar and coal-based activated carbon, respectively. The pore size of the surface-engineered biochar also decreases with higher CTAB concentrations, ranging from 1148–1190 nm for PKS-1CMC to 1162–1177 nm for PKS-1.5CMC and 993–1018 nm for PKS-2CMC. The reduction in pore size suggests that CTAB was successfully deposited onto the biochar surface, narrowing the pores and indicating effective surface modification.

The FTIR spectra of biochar samples in Fig. 2(e) show only minor differences between the unmodified and surface-engineered biochar. The spectra were compared with the literature for identification of surface functional groups [52–56]. A small peak can be seen at 3457 cm^{-1} corresponding to O–H stretching, indicative of water or hydrogen-bonded hydroxyl group. Multiple peaks between 2800 – 3050 cm^{-1} can be attributed to symmetric and asymmetric stretching of C-H_x that belong to the aliphatic CH_x group. An intense sharp peak at 1758 cm^{-1} is

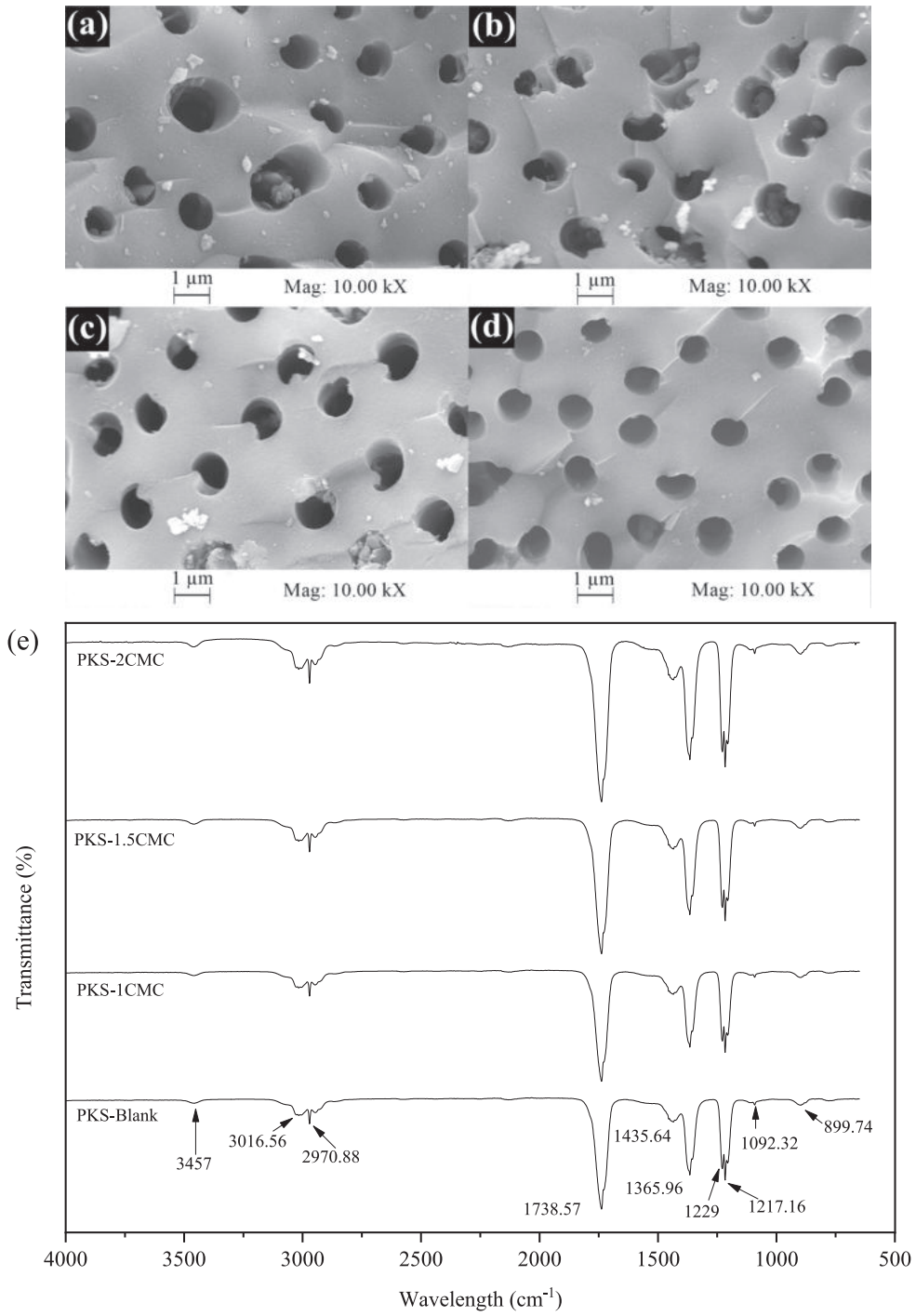

Fig. 2. FESEM micrographs of (a) PKS-Blank, (b) PKS-1CMC, (c) PKS-1.5CMC, (d) PKS-2CMC and (e) FTIR spectra of all biochar samples.

characteristic of C=O stretching of the carbonyl group, while a broad peak at 1535 cm^{-1}, which overlapped with adjacent peaks, can be ascribed to C=C and C=O of aromatic compounds. A long peak between 1350–1425 cm^{-1} suggests the presence of C–H bending vibrations of the CH_x group. Collective peaks between 1200 – 1300 cm^{-1} emerge due to C–C skeletal vibration, while a minor peak at 1092 cm^{-1} represents symmetric stretching of C-O-C in aryl–alkyl ethers. In addition, a small peak at 899 cm^{-1} reflects the existence of C–H bending from aromatic C–H out-of-plane deformation. The introduction of CTAB onto the biochar is evidenced by increased transmittance intensities at 1090 – 1360 cm^{-1}, 1450–1600 cm^{-1} and 2800–3050 cm^{-1} ranges, corresponding to increasing CTAB concentrations. This trend aligns with the findings from the previous studies. An enhancement in the intensity around 1090 – 1360 cm^{-1} is attributed to the C-N vibration of the amine group in the polar head of the CTAB molecule [57]. On the other hand, the increased intensities at 1450–1600 cm^{-1} and 2800–3050 cm^{-1} can be linked to the increment in C-H_x symmetric and asymmetric vibrations of the methyl chain in CTAB's non-polar tails [58].

The FESEM micrographs in Fig. 3(a)–(e) verify the characteristics of MP and NP samples described in Section 2.2. PE40-48 and PE2-4 show similar morphologies, consisting of numerous rough clumps forming nearly spherical shapes, similar to the MP and NP samples studied by Pulido-Reyes et al. [22]. As neither sample exhibits a perfect spherical shape, they are classified as irregular-shaped MP. It should be noted that

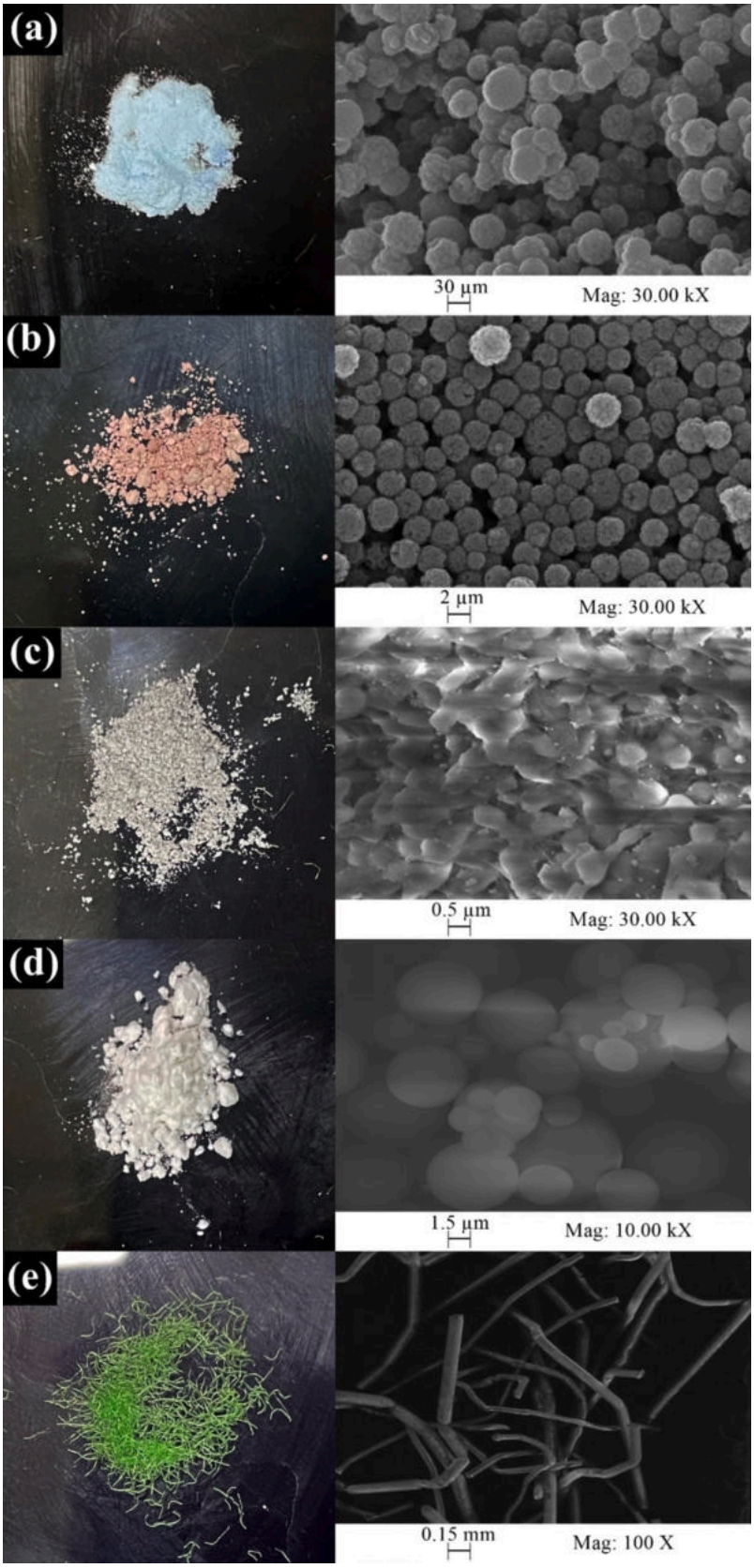

Fig. 3. Raw image and FESEM micrographs of (a) PE40-48, (b) PE2-4, (c) PENano, (d) PA6-9 and (e) PAFibre.

Table 2
Zeta potential and contact angle measurements of all biochar and MP and NP samples.

Sample	Zeta potential (mV) at pH = 7	Water droplet's contact angle
PKS-Blank	− 18.3	112.6°
PKS-1CMC	+ 9.5	118.2°
PKS-1.5CMC	+ 12.9	120.2°
PKS-2CMC	+ 14.1	117.3°
PE40-48	− 29	121.2°
PE2-4	− 38.2	120.7°
PA6-9	− 36.6	117.2°
PAFibre	− 50.1	129.4°
PENano	− 45.7	128.4°

both samples show a tendency to agglomerate, which is evident in both their raw images and FESEM micrographs in Fig. 3(a) and (b). PENano, shown in Fig. 3(c), also tends to form agglomerates, and no distinct shape can be defined for the individual particles. This behaviour is characteristic of nanoparticles, which often aggregate due to surface effects. PA6-9 particles, shown in Fig. 3(d), exhibit a perfectly spherical shape with a very smooth surface. Nonetheless, the particle sizes observed in the micrograph differ from the data provided by the supplier, with some particles even smaller than 1 μm. In addition, it should be noted that the actual colours of PENano and PA6-9 are grey and white, respectively, allowing particle differentiation during inspection in the lab. PAFibre, depicted in Fig. 3(e), shows a smooth morphology similar to its raw image, possibly because of its large particle size.

A negative zeta potential value (−18.3 mV) as measured for PKS-Blank (Table 2) indicates that its surface is predominantly covered with negatively charged compounds. This arises due to the reduction of oxygen-containing groups during pyrolysis, which deoxygenates the biochar surface [59]. Upon modification with CTAB, the zeta potential shifts to positive values ranging from +9.5 to +14.1 mV, in an increasing trend with increased CTAB concentration. The change in zeta potential is attributed to the alkylammonium cations present in the hydrophilic polar head of CTAB, which are intercalated or adsorbed onto the biochar surface, neutralizing the available negative charges and imparting a positive charge [60]. The water-droplet contact angle measurements demonstrate that all biochar samples exhibit hydrophobic properties, which are further increased with CTAB modification. PKS-Blank possesses high hydrophobicity, most likely due to the pyrolysis process reducing the presence of functional groups such as carbonyl and ethyl, while simultaneously forming more hydrophobic groups such as phenol, pyridine and lactone [61,62]. The most significant increase in hydrophobicity is observed in PKS-1.5CMC, with a water droplet contact angle of 120.2°, suggesting that the long non-polar tails of CTAB, were adsorbed and compacted on the biochar surface, increasing its hydrophobicity [63]. In the context of MP and NP, all samples are inherently hydrophobic with highly negative zeta potential as a result of their long non-polar hydrocarbon chains. These surface properties are expected to play a crucial role in the removal of MP and NP by both the unmodified and surface-engineered biochar. This will be discussed further in the upcoming subsections.

3.2. MP removal by surface-engineered biochar

The performance of unmodified and surface-engineered biochar in removing PE2-4 from aqueous solutions via filter-media-based filtration was investigated using turbidity and gravimetric methods. The turbidity removal data collected at every 5-minute interval within 2 h of experiments are as shown in Fig. 4, representing PE2-4 removal efficiencies by biochar samples modified with different CTAB concentrations. The overall performance measured by both turbidity and gravimetric methods and the observed biochar bed depth reached by PE2-4 are summarised in Table 3. The percentage of MP removal reported in Table 3 is the maximum PE2-4 removal achieved during the experiment.

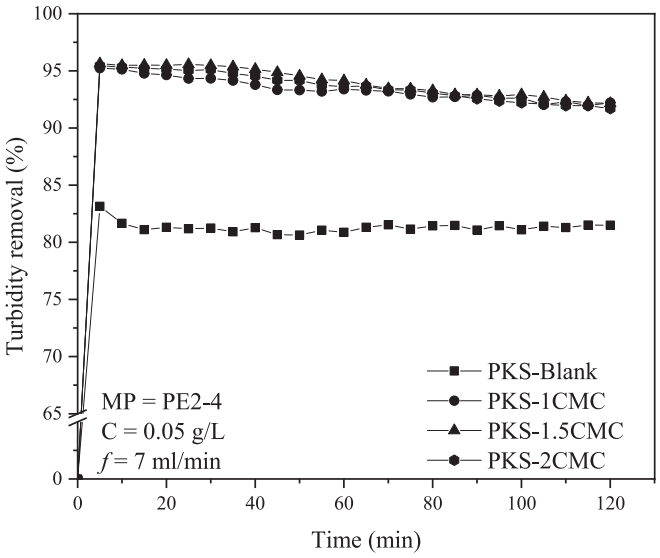

Fig. 4. PE2-4 removal trends measured via turbidity method by unmodified biochar and surface-engineered biochar modified with different CTAB concentrations.

Table 3
PE2-4 maximum removal efficiency by unmodified and surface-engineered biochar of different CTAB concentrations measured using turbidity and gravimetric methods and the observed bed depth reached by MP.

Sample	MP removal (%)		Bed depth reached by MP particles (cm)
	Turbidity method	Gravimetric method	
PKS-Blank	83.54	84.40	6
PKS-1CMC	95.28	94.87	2
PKS-1.5CMC	95.71	96.13	2.5
PKS-2CMC	95.45	95.13	4

Table 3 reveals that filtration using unmodified biochar can achieve up to 84 % PE2-4 removal efficiency as measured by turbidity and gravimetric methods. The removal efficiency is significantly enhanced to over 94 % using surface-engineered biochar, irrespective of CTAB concentration. These results are consistent with the findings by Shen et al. [20], which reported that modifying filter media with cationic surfactants leads to significant enhancement of MP removal in filtration process. In addition, the surface-engineered biochar samples reduce the biochar bed depth reached by PE2-4 particles to between 2–4 cm, in comparison to the unmodified sample (PKS-Blank), where particles can be visually observed as deep as 6 cm. This implies that most plastic particles are immobilized at the upper layer of the surface-engineered biochar bed. Prolonging the MP removal process forms a filter cake layer, which can be visually observed through the glass column. The thickness of the filter cakes also correlates with the bed depth reached, where thicker cakes are observed for samples with shorter bed depth reached by the MP particles. All surface-engineered biochars show similar MP removal efficiencies around 95 %, however, the highest performance is demonstrated by PKS-1.5CMC based on turbidity and gravimetric measurements. The overall MP removal efficiency follows the order: PKS-1CMC < PKS-2CMC < PKS-1.5CMC.

PKS-1.5CMC, identified as the optimal sample, was further tested for removal of MP and NP particles of different sizes, shapes and polymer types, including PE40-48, PE2-4, PA6-9, PAFibre and PENano, as well as the mixture of these particles (MIX). The removal performance demonstrated by PKS-1.5CMC was compared against the unmodified biochar sample (PKS-Blank) in Fig. 5 and Table 4. Fig. 5(a)–(f) show MP

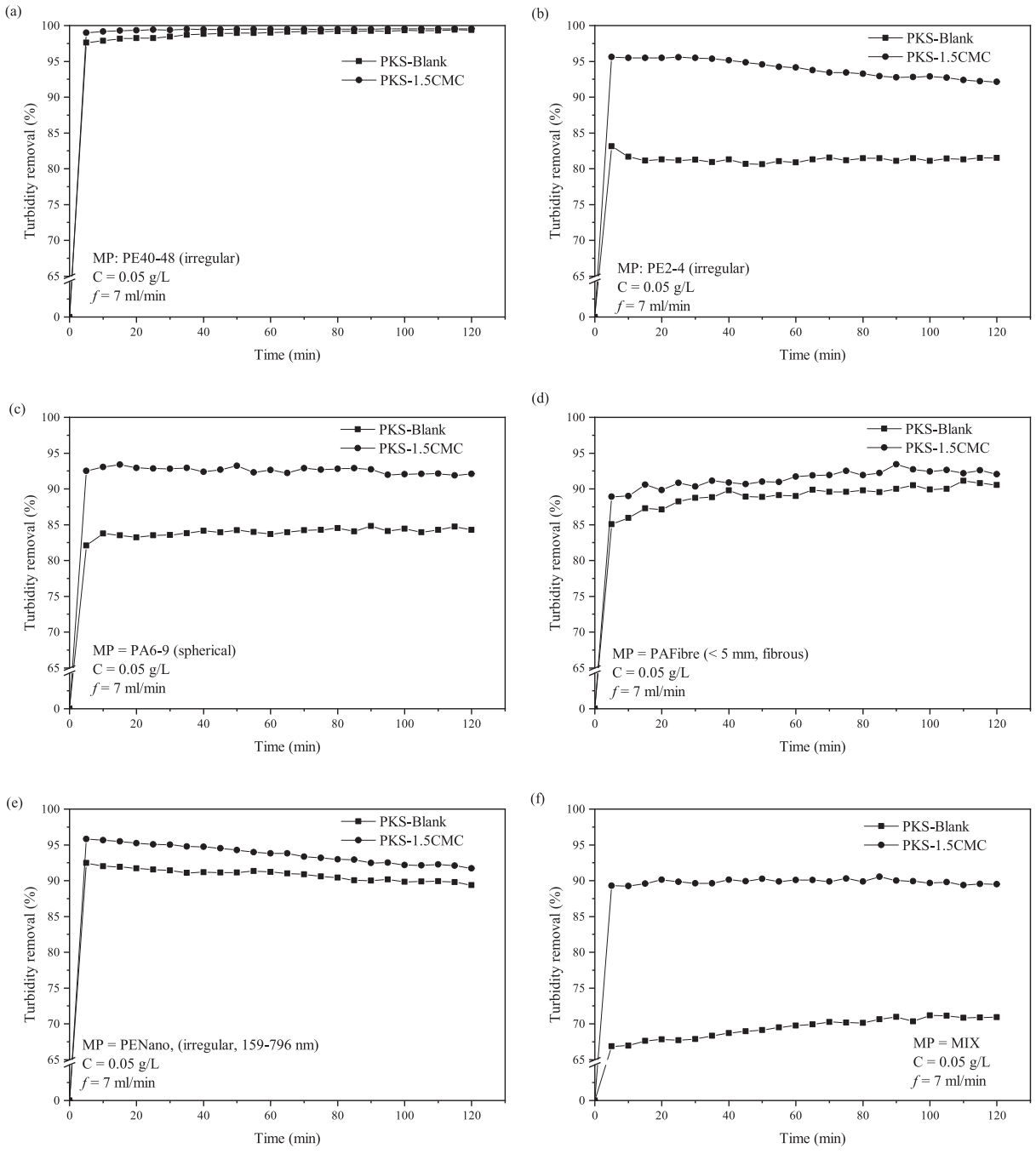

Fig. 5. Comparison of MP and NP removal trends measured by turbidity method using PKS-Blank and PKS-1.5CMC: (a) PE40-48, (b) PE2-4, (c) PA6-9, (d) PAFibre, (e) PENano and (f) MIX.

and NP removal trends across the different samples, measured by the turbidity method at every 5-minute interval within a 2-hour experiment, while Table 4 summarises the maximum removal achieved during experiments by both turbidity and gravimetric measurements and the observed bed depth reached by the MP and NP particles.

The study on the removal of various MP and NP particles further proves the superiority of PKS-1.5CMC, which consistently outperforms PKS-Blank in all samples tested. While PKS-Blank can remove more than 90 % of MP and NP for three of the samples, i.e., PE40-48, PAFibre and PENano, as measured via turbidity and gravimetric methods, it demonstrates lower removal efficiency (< 87 %) for the remaining samples, with the lowest performance observed for the MIX sample (< 72 %). In contrast, PKS-1.5CMC exhibits superior performance across all MP and NP particles tested, highlighting the importance of an appropriately engineered surface charge for effective MP and NP removal. All tested samples exhibit negative zeta potential values at the pH used in this study (pH = 7). This reinforces the conclusion that strong electrostatic attraction between the negatively charged particles and the positively charged PKS-1.5CMC is a key factor in achieving high removal efficiencies.

PKS-1.5CMC also effectively limits the movement of MP and NP particles through the filter media bed, except for PAFiber, where the same travel depth was observed for both PKS-1.5CMC and PKS-Blank. PE2-4 particles travel deepest in both filter media, with detection up to 6 cm in PKS-Blank and 2.5 cm in PKS-1.5CMC. This results in the formation of thicker filter cakes on the PKS-1.5CMC biochar bed

Table 4
Summary of MP and NP removal efficiencies by PKS-Blank and PKS-1.5CMC measured via turbidity and gravimetric methods and the observed bed depth reached by different MP and NP particles.

Sample	PKS-Blank			PKS-1.5CMC		
	MP and NP removal (%)		Bed depth reached by MP and NP (cm)	MP and NP removal (%)		Bed depth reached by MP and NP (cm)
	Turbidity method	Gravimetric method		Turbidity method	Gravimetric method	
PE40-48	99.44	99.13	1.25	99.61	99.40	1
PE2-4	83.54	84.40	6	95.71	96.13	2.5
PA6-9	85.24	86.33	4	93.64	95.00	2
PAFibre	91.50	92.07	0.2	93.66	94.53	0.2
PENano	92.45	92.33	2.25	95.83	95.07	1.5
MIX	71.31	69.67	2.75	90.90	90.33	1

compared to PKS-Blank, similar to the results obtained in the previous section. Additionally, it should be noted that tiny biochar powdered particles may be carried into the effluent due to the continuous water flow, causing an underestimation of the removal efficiencies by turbidity and gravimetric methods. Microscopic observation of the filter paper used to filter the collected effluent confirms the presence of these small biochar particles, indicating that the reported value in Table 4 is slightly underestimated. Although PKS-1.5CMC significantly enhanced the removal of all tested MP and NP particles, notable differences in the removal performance are observed among samples. The differences are likely due to the variations in particle size, shape, and polymer type in the MP and NP samples. The lowest removal efficiency for the MIX sample can be attributed to the combined negative effects of all these factors acting simultaneously.

The enhancement in MP removal efficiency by surface-engineered biochar is largely attributed to the modifications in biochar surface properties, especially the zeta potential and hydrophobicity, as previously highlighted in the sample characterization. The introduction of CTAB increases biochar hydrophobicity and shifts its surface charge from negative to net positive. The increase in hydrophobicity of the biochar allows stronger interaction between the surface-engineered biochar and the hydrophobic MP particles through hydrophobic interaction, resulting in the immobilization of MP and the formation of hydrophobic aggregates, consistent with a previous finding by Ivanic et al. [64]. A similar observation on the interaction between hydrophobic filter media and MP particles was reported by Gao et al. [65], though under different experimental conditions. In the context of zeta potential, the poor MP removal exhibited by PKS-Blank can be explained by electrostatic repulsion, as both the MP particles and PKS-Blank possess net negative surface charge. The introduction of cationic CTAB onto the biochar surface results in a net positive charge, facilitating immobilization of the negatively charged MP particles. In accordance with our findings, previous studies by Ganie et al. [66] and Yen et al. [67] also demonstrated that MP and NP removal can be significantly enhanced when the biochar and MP and NP particles have opposite charges, which enable electrostatic attraction.

It should be emphasized that the concentration of CTAB also plays an important role in the effectiveness of surface-engineered biochar for MP removal. The structure of CTAB and the potential aggregation of surfactant molecules are shown in Fig. 6. CTAB is a cationic surfactant with a positively charged polar hydrophilic head and a negatively charged non-polar hydrophobic tail [35]. During the surface modification process, the positively charged hydrophilic head of the CTAB molecule attaches to the negatively charged biochar surface via electrostatic attraction. At a concentration below CMC, CTAB forms a hemimicelle structure, which is unsuitable for MP removal as the negatively charged hydrophobic tails are oriented outward. This results in electrostatic repulsion between the CTAB-modified biochar and the negatively charged MP and NP particles [51,68], reducing the removal efficiency. Therefore, achieving an optimal CTAB concentration is critical to ensuring surface modification enhances electrostatic attraction and promotes efficient MP and NP removal.

As the CTAB concentration approaches and exceeds the CMC, CTAB molecules aggregate into an admicelle structure, with the positively

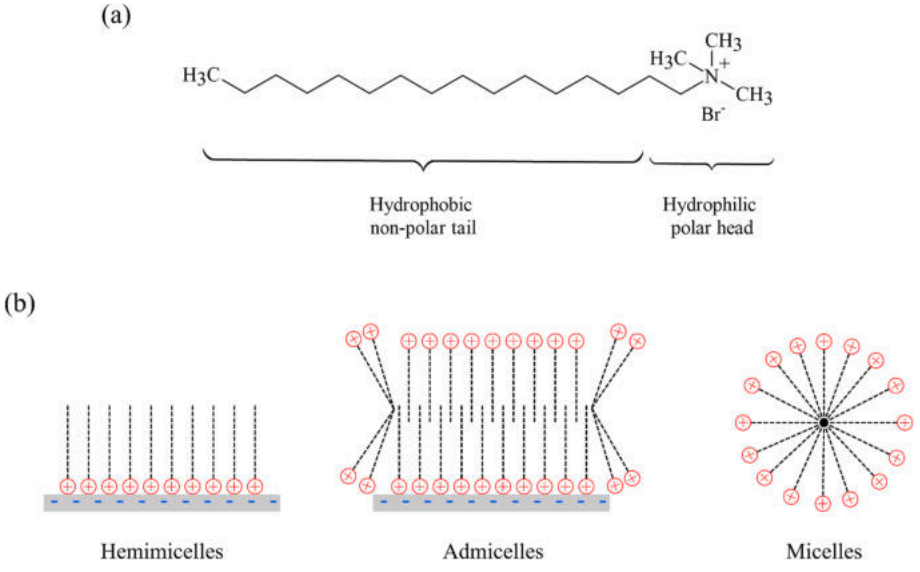

Fig. 6. (a) Structure of CTAB and (b) Possible aggregation structure of CTAB particles.

charged hydrophilic heads in the outward position [69]. This arrangement enables electrostatic attraction between the MP and NP particles and the surface-engineered biochar, resulting in their retention on the biochar surface. A higher concentration of CTAB facilitates the formation of more admicelles on the biochar surface, thus increasing MP retention, as observed in PKS-1.5CMC compared to PKS-1CMC. However, excessive CTAB concentration reduces MP removal efficiency, as observed in PKS-2CMC. This decline occurs because, at very high concentrations, admicelles begin forming in the CTAB solution itself rather than on the biochar surface [51]. Consequently, fewer admicelles interact with the biochar surface, resulting in lower biochar capacity for MP removal. The phenomenon is consistent with findings from other studies, e.g., Nagireddi [57], who reported that optimal removal of heavy metals was achieved at an optimal CMC.

3.3. Influence of MP and NP properties on removal performance

The previous section demonstrated that the removal efficiencies of MP and NP samples using surface-engineered biochar vary significantly due to the influence of particle properties such as size, shape and polymer type. In the context of MP and NP sizes, no clear correlation was observed between particle size and removal efficiency. The removal efficiencies of different MPs by PKS-1.5CMC followed the order: PE40-48 > PENano ≈ PE2-4 > PAFibre ≈ PA6-9 > MIX for the turbidity method and PE40-48 > PE2-4 > PENano ≈ PA6-9 > PAFibre > MIX for the gravimetric method. The mobility of MP and NP particles through the filter media bed can be represented by the ratio of MP or NP diameter and filter media diameter ($d_{MP/NP}/d_{FM}$). According to Gao et al. [65], the ratio provides an insight into particle behaviour as follows: (i) $d_{MP/NP}/d_{FM} < 0.11$ refers to conditions where particles move freely through the filter media, (ii) $0.11 < d_{MP/NP}/d_{FM} < 0.32$ corresponds to limited particle movement through the filter media, and (iii) $d_{MP/NP}/d_{FM} > 0.32$ corresponds to the retainment of particles on the surface of filter media. All MP and NP samples, except PAFibre, fall into category (i), where particles are expected to move freely through the filter media. PAFibre, with a significantly higher $d_{MP/NP}/d_{FM}$ value of 3.3708, indicates greater retention on the surface of the filter media.

Even though larger MP particles can move freely through the filter media, more than 99 % removal is still achieved for PE40-48, even by PKS-Blank, as the filter media can easily trap these larger-sized MP within the pores and on the surface of the filter media bed. Taking into account the underestimation of results discussed previously due to the presence of small biochar particles, it can be considered that the filtration system almost entirely removes PE40-48. This is consistent with the literature, which reported a high removal efficiency for MP particles larger than 20 μm through filtration [18][48]. Smaller $d_{MP/NP}/d_{FM}$ values are obtained with smaller MP and NP particles, implying that they can penetrate the filter bed media easily and get discarded in the effluent, thus reducing the removal efficiencies [22]. Interestingly, although PA6-9 has a larger theoretical size and $d_{MP/NP}/d_{FM}$ value compared to PE2-4, the latter achieves higher removal efficiency. A closer inspection of the particle size distribution, as observed in the FESEM micrographs in Fig. 3(d), provides an insight into this discrepancy. The PE2-4 particles can be considered uniformly distributed as they are more uniform in size, with all particles falling well within the size range provided by the supplier. On the other hand, PA6-9 has a broader particle size distribution, with some particles smaller than 1 μm. These smaller PA6-9 particles likely have a much lower actual $d_{MP/NP}/d_{FM}$ value, allowing them to pass through the biochar bed more easily, making the removal efficiency of PA6-9 lower in comparison to PE2-4.

A significant reduction in $d_{MP/NP}/d_{FM}$ is observed when the plastic particles are further reduced to nano-size, suggesting ease of NP particle movement through the filter media bed. Therefore, the removal efficiency of PENano is expected to be the worst among all the studied samples. However, contrary to the expectation, PENano displays a better removal efficiency than several larger-sized MP samples. This can be attributed to nanoparticle agglomeration, which leads to the formation of larger clumps of plastic particles, as seen in the FESEM micrographs in Fig. 3(c) [70]. Agglomeration occurs due to the high energy possessed by PENano, which causes particles to attract each other through weak forces, e.g., van der Waals interactions or adsorbed onto surrounding elements. This reduces their Gibb's free energy until equilibrium is reached [71]. As a result of this agglomeration, the average particle size increases, causing PENano to be more easily retained by PKS-1.5CMC. This result aligns with the findings by Ramirez Arenas et al. [72] and Pulido-Reyes et al. [22], who reported that NP removal via filtration is enhanced when particles agglomerate naturally or with the assistance of a coagulant. On the other hand, the highest removal efficiency is expected for PAFibre due to its high $d_{MP/NP}/d_{FM}$ value, which suggests that these fibrous particles can be easily immobilized on the surface of the filter media upper layer [73]. This is consistent with the findings in this study where PAFibre is only detected at the top 0.2 cm of the filter media bed, even with the utilization of PKS-Blank, as summarized in Table 4. However, the overall removal performance of PAFibre is lower than that of other MP and NP particles, possibly due to the shape and smoothness of the fibres. These characteristics reduce the likelihood of effective filtration, as fibres may exhibit lower adhesion to the filter media surface despite their large size and limited mobility.

The removal efficiency of the MP and NP samples, as summarized in Table 4, follows the trend: irregular > spherical > fibre. The higher removal efficiencies exhibited by irregular MP and NP particles (PE40-48, PE2-4 and PENano) can be linked to their lower mobility through the filter media. These particles are more likely to become entangled with the biochar filter media, and their rough surfaces enhance immobilization by fitting into the grooves and pores of the biochar bed. This suggests that shape irregularity and surface roughness are among critical factors in particle retention, as they facilitate stronger interaction with the filter media, resulting in higher removal efficiencies than spherical or fibrous particles. Similar findings were observed by Rullander et al. [74], who reported that irregularly shaped plastic particles achieved the highest retainment in horizontal flow sand filters compared to spherical and fibrous particles. This is especially relevant because irregularly shaped particles make up the majority of MP and NP in the environment. Therefore, the high removal performance demonstrated for irregular particles in this study is highly beneficial for achieving effective MP and NP removal in real-world applications.

The lower removal efficiency observed for PA6-9 and PAFibre is primarily attributed to their spherical and fibrous morphologies and smooth surfaces, as shown in the FESEM micrographs in Fig. 3(d) and 3 (e). The smooth surfaces result in higher mobility throughout the filter bed, reducing the tendency to be immobilized by the filter media. In the case of spherical particles like PA6-9, various MP and NP-related studies [32,75,76] have similarly reported that these particles exhibit high mobility and can be easily passed through the filter media. The high mobility of spherical particles can be attributed to (i) lacking of sharp edges or angles, resulting in minimal point of contact with filter media, making them less likely to become trapped within the pores, (ii) having a low surface-area-to-volume ratio, which minimizes the drag and resistance experienced by these particles, enabling smoother passage through the filter bed, and (iii) having a symmetrical shape which results in consistent forces on the surface of the particles, ensuring uniform motion and preventing erratic movements that might otherwise lead to entrapment within the filter media. These characteristics combined contribute to the lower retention of PA6-9 and PAFibre, reflecting the importance of particle morphology in filtration-based MP and NP removal.

In the context of fibrous particles, e.g., PAFibre, their retention is also highly dependent on the orientation of the particles as they move through the filter media bed [74]. Fibres are characterised by having one dimension (length) considerably larger than the other (width or thickness). When the movement of fibrous particles is aligned with their larger dimension, they are more easily retained on the upper layer of the

filter media. This is observed for most PAFibre particles in the study, as their movement through the filter bed is significantly hindered, with the deepest penetration reaching only 0.2 cm. Nonetheless, some fibrous particles may orient themselves along their smaller dimension as they traverse through the filter bed, allowing them to move longitudinally. This facilitates higher particle mobility through the filter media, enabling some fibres to escape the filter bed, thereby reducing the overall removal efficiency [77,78]. This dynamic of alternating between restricted and unimpeded movement based on orientation highlights the challenge of fully capturing fibrous particles using filtration methods, particularly in systems relying on mechanical entrapment alone. This emphasizes the need for enhanced filtration strategies, such as using surface-engineered biochar or adjusting filtration parameters, to improve the removal of fibrous microplastics.

In this study, two polymer types were examined, polyethylene (PE) and polyamide (PA), where higher removal efficiency can be observed for the PE-based samples (PE40-48, PE2-4 and PENano) compared to the PA-based samples (PA6-9 and PAFibre). Although the polymer type can significantly affect the retention of suspended particles, primarily due to differences in density, this effect is deemed negligible in this study. Both polymers have densities that are very close to water density (polyethylene = 0.91–0.94 g/cm^3, polyamide = 1.01 g/cm^3), which minimizes the influence of gravitational forces on the removal process [65]. This is supported by Rullander et al. [74], who studied the removal of PE, PA and polyethylene terephthalate (PET) based MPs using sand as the filter media. They reported that only PET particles were highly retained due to their significantly higher density (1.35 g/cm^3) than water, whereas PE and PA particles, with densities similar to water, exhibited less retention by the filter media. This reinforces the importance of understanding the physical and chemical properties of plastic particles, beyond just polymer type, in influencing their interaction with filtration media, especially when considering the design of engineered filters.

As the density effect is negligible, the difference in the removal performance of PE and PA-based MPs is likely attributed to the difference in their hydrophobicity and zeta potential. As discussed earlier, the electrostatic attraction between positively-charged PKS-1.5CMC and negatively-charged MP and NP particles can enhance the MP and NP removal process [79]. Additionally, hydrophobic interactions play a significant role in improving removal efficiency, especially for more hydrophobic particles [64]. As shown in Table 4, the samples used in this study follow the order of PE40-48 > PA6-9 > PE2-4 > PENano > PAFibre in zeta potential and PAFibre > PENano > PE40-48 > PE2-4 > PA6-9 in hydrophobicity. The difference in zeta potential and hydrophobicity of each MP and NP sample results in different strengths of interaction with PKS-1.5CMC filter media. The higher hydrophobicity and zeta potential of PE-based samples enable stronger interactions with the biochar, resulting in higher retention than PA-based samples. Additionally, other factors mentioned earlier, such as shape and surface roughness, affect PA-based samples, reducing their removal efficiency. The finding aligns with the results reported by Rullander et al. [74], who also observed a higher amount of PA particles in the filtration effluent compared to PE particles.

3.4. Possible removal mechanism

Based on the findings of this study and supporting literature, the removal mechanism of MP and NP particles by CTAB-modified biochar filter media can be clarified. Filtration mechanism plays a pivotal role in the removal process, as proposed by Wang et al. [31] and corroborated by related studies [20,23,24,25,80,81]. During filtration, the retention of MP and NP particles may occur in several ways: (i) being stuck (blinded) in between the filter media due to size exclusion, (ii) entanglement with small chips or particles of the filter media, particularly for those with irregular shapes or fibrous forms, and, (iii) adhesion onto the filter media surface due to electrostatic attraction or hydrophobic interactions between MP and NP particles and the biochar surface. The fourth mechanism proposed in some studies, entrapment inside filter media pores, is unlikely to happen in this study. The MP and NP particles used are larger than the typical pore size of CTAB-engineered biochar, making it impossible for them to be trapped within the biochar surface pores.

Since filtration is proposed as the dominant mechanism for the retention of MP and NP by biochar in this study, conventional adsorption-related mechanisms, e.g., adsorption breakthrough models like Thomas, Yoon-Nelson, Adams-Bohart etc.), adsorption kinetics (pseudo-first order, pseudo-second order etc.) and adsorption isotherms (Freundlich, Langmuir etc.) usually applied in activated carbon adsorption studies are not applicable for explaining the MP and NP removal process. This is true because these models are typically used to describe solute adsorption onto adsorbent surfaces, whereas, in this study, MP and NP particles are physically retained through filtration-based mechanisms. The possible removal mechanisms of MP and NP in this study discussed earlier are illustrated in Fig. 7, comprising MP sticking between biochar packing, entanglement with small biochar particles, adhesion on biochar grooves, electrostatic interaction, hydrophobic interaction and filter cake formation. Filter cake formation happens due to the accumulation of particles on the surface of the filter media, creating a filter cake which can further improve retention by blocking the media pores and trapping additional particles. These mechanisms collectively contribute to the efficient removal of MP and NP from the solution during filtration with the surface-engineered biochar.

The tightly packed biochar bed inside the filtration column plays a key role in retaining MP and NP particles, where particles smaller than the gap between the biochar particles can pass through, as noted by Palansooriya et al. [82]. For example, MP particles such as PE40-48 are easily blinded between the filter media due to their large average size, resulting in immobilization and high removal efficiency. Similarly, NP agglomeration also leads to an increase in their particle size, enhancing their immobilization by the filter media. Smaller-sized MP particles, however, are more challenging to retain. Due to their smaller dimensions, a portion of these particles can penetrate the biochar bed and exit with the filtration water permeate. Despite this, many MP and NP particles are ‘blinded’ and occupy the spaces between biochar particles. As more particles flow into the column, these blinded particles block the gaps between biochar, preventing subsequent particles from passing through and are immobilized on the upper layer of the biochar bed as a filter cake layer [83]. The filter cake formation is initially beneficial in facilitating the retention of additional MP and NP particles. However, as filter cake thickens, it may cause a pressure drop within the system, resulting in slower filtration and reduced water flow inside the column, eventually compromising the overall filtration performance [84]. Therefore, while beneficial in the short term, excessive filter cake formation can be detrimental to the long-term effectiveness of the filtration process.

The formation of small biochar particles or chips inside the filtration column due to disintegration from particle collisions or the continuous water flow is a notable factor in the retention of MP and NP particles. As MP and NP particles pass through the filtration column, they may become entangled with these smaller biochar particles or chips, facilitating their retention on the biochar surface [23]. This entanglement can also lead to particle enlargement, aiding in the subsequent filtration by the filter media [85]. The effectiveness of the adhesion process is highly dependent on the surface properties of biochar. Biochar with a rougher surface, characterised by numerous grooves, provides more attachment sites for the MP and NP particles, enhancing retention [25]. This effect is observed in our previous study [43], where palm kernel shell biochar, which possesses a higher surface roughness, exhibits superior MP retention in comparison to coconut shell biochar. The increased surface roughness allowed for more opportunities to become immobilized, demonstrating that biochar roughness plays a critical role in the

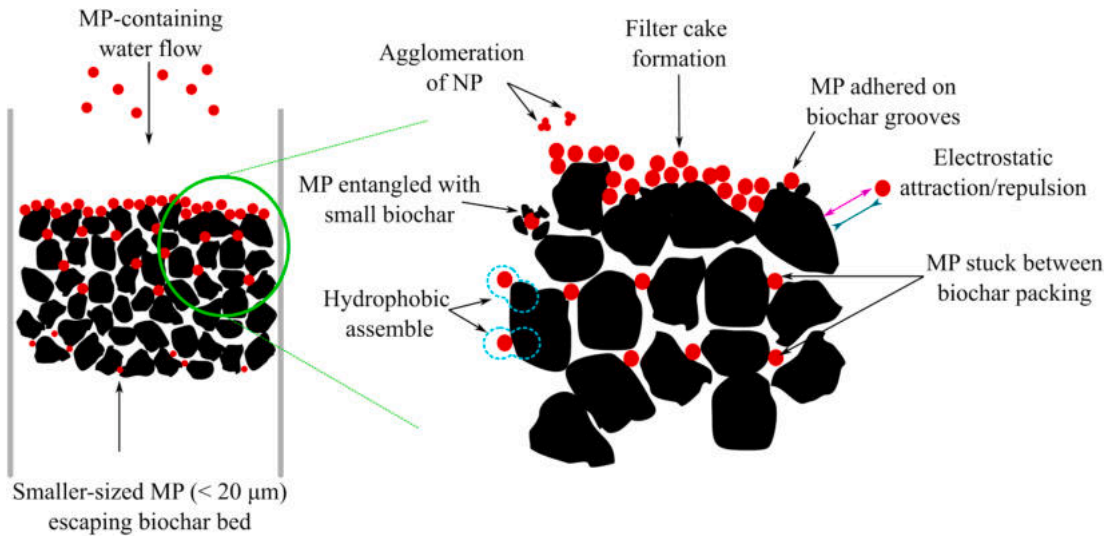

Fig. 7. Possible MP and NP removal mechanisms by filter media-based filtration.

filtration-based removal of MPs and NPs. This finding supports the broader conclusion that both the biochar properties (such as surface roughness) and the physical dynamics within the filtration column (e.g., biochar disintegration and particle entanglement) are crucial factors in determining the overall efficacy of the MP and NP removal process.

The adhesion of MP and NP particles is also driven by various interactions such as electrostatic interaction, hydrophobic interaction, π-π interaction and hydrogen bonding. When unmodified biochar (PKS-Blank) is used, both the biochar and MP/NP particles exhibit a negative surface charge, resulting in electrostatic repulsion, which reduces the removal performance, as reported by Li et al. [25]. However, the biochar modified with CTAB gains a positive surface charge, which allows electrostatic attraction with the negatively charged MP and NP particles, significantly enhancing removal efficiency [20]. Since all biochar, MP, and NP particles in this study are hydrophobic, they can adhere to each other through hydrophobic interactions. These interactions form hydrophobic aggregates, which repel the surrounding water, facilitating the retention of MP and NP particles on the biochar surface [64]. When aromatic groups are present, removing MP and NP via π-π interaction is common in filtration studies. However, this mechanism is not relevant to this study because both PE and PA particles used do not contain aromatic groups, which are necessary for such interactions to occur. In addition, hydrogen bonding is unlikely to play a significant role as the hydrogen atoms on PE molecules are not attached to electronegative atoms, which reduces the potential hydrogen bonding with the biochar surface. Although PA could theoretically form hydrogen bonding with biochar due to the presence of nitrogen and oxygen atoms in the polyamide structure, this mechanism appears insignificant to other removal mechanisms in this work. The lower removal of PA-based MP in this study compared to PE suggests that hydrogen bonding is not a dominant removal mechanism. In summary, the dominant mechanisms in this study are electrostatic and hydrophobic interactions, with electrostatic forces enhanced by the biochar modification with CTAB, while π-π interaction and hydrogen bonding have minimal to negligible impact on MP and NP removal.

4. Conclusion

This study investigates the effectiveness of PKS-biochar modified with CTAB for enhancing the removal efficiency of MP and NP from aqueous solutions. The surface modification significantly improves the biochar properties, resulting in a net positive surface charge and increased hydrophobicity. These changes facilitate stronger interactions between MP/NP particles and the surface-engineered biochar through electrostatic attraction and hydrophobic interaction. The removal of MP and NP does not only depend on the properties of the biochar but is also highly dependent on the properties of MP and NP particles, such as size, shape and polymer type. In general, smaller-sized particles exhibit lower removal efficiency due to their high mobility within the filter media. However, NP particles demonstrate high removal efficiency due to their tendency to agglomerate, resulting in larger particle sizes that enhance retention. In addition, irregularly shaped MP and NP show higher removal efficiency due to their ability to become immobilized within the grooves and pores of the biochar bed. This contrasts with spherical and fibrous shapes, which possess smoother surfaces that facilitate movement through the biochar bed, leading to lower removal efficiency. PE-based MP and NP particles exhibit higher removal efficiency than their PA-based counterparts. This difference can be attributed to PE's relatively less negative surface charge and higher hydrophobicity, which result in stronger interactions with the surface-engineered biochar. The modification of biochar with CTAB has proven effective in improving the removal of MP and NP from water, highlighting the potential for enhanced performance in mitigating pollution. However, further research is recommended to assess the practical application and the effectiveness of surface-engineered biochar in real-world scenarios and large-scale applications. This will help determine its viability as a sustainable solution for addressing MP and NP pollution in aquatic environments.

CRediT authorship contribution statement

Muhammad Adli Hanif: Investigation, Methodology, Validation, Data curation, Visualization, Writing – original draft. **Naimah Ibrahim:** Conceptualization, Supervision, Funding acquisition, Resources, Writing – review & editing. **Nur Adlyna Hayazi:** Investigation. **Farrah Aini Dahalan:** Supervision, Writing- Reviewing and Editing. **Umi Fazara Md. Ali:** Supervision, Writing- Reviewing and Editing. **Aishah Abdul Jalil:** Resources, Writing- Reviewing and Editing. **Achmad Syafiuddin:** Writing- Reviewing and Editing.

Declaration of competing interest

The authors declare that they have no known competing financial interests or personal relationships that could have appeared to influence the work reported in this paper.

Acknowledgements

The authors acknowledge the financial support provided by the Ministry of Higher Education Malaysia through the Fundamental Research Grant Scheme (FRGS) under grant number FRGS/1/2020/WAB02/UNIMAP/02/1 and Universiti Malaysia Perlis for postdoctoral funding (9001-00790).

Data availability

Data will be made available on request.

References

[1] R.Y. Krishnan, S. Manikandan, R. Subbaiya, N. Karmegam, W. Kim, M. Govarthanan, Recent approaches and advanced wastewater treatment technologies for mitigating emerging microplastics contamination – A critical review, Sci. Total Environ. 858 (2023) 159681, https://doi.org/10.1016/j.scitotenv.2022.159681.

[2] B. Xia, Q. Sui, Y. Du, L. Wang, J. Jing, L. Zhu, X. Zhao, X. Sun, A.M. Booth, B. Chen, K. Qu, B. Xing, Secondary PVC microplastics are more toxic than primary PVC microplastics to Oryzias melastigma embryos, J. Hazard. Mater. 424 (2022) 127421, https://doi.org/10.1016/j.jhazmat.2021.127421.

[3] T.Y. Hwi, Y.S. Ibrahim, W.M. Khalik, W.m. A, Microplastic abundance, distribution, and composition in sungai dungun, terengganu, Malaysia. Sains Malaysiana 49 (7) (2020) 1479–1490.

[4] R.N. Raja Sulaiman, A. Abu Bakar, N. Ngadi, I.N. Shamsul Kahar, A.H. Nordin, M. Ikram, W. Nabgan, Microplastics in Malaysia' s aquatic environment: current overview and future perspectives, Global Chall. 7 (2023) 2300047, https://doi.org/10.1002/gch2.202300047.

[5] S. Ghosh, J.K. Sinha, S. Ghosh, K. Vashisth, S. Han, R. Bhaskar, Microplastics as an emerging threat to the global environment and human health, Sustainability (Switzerland) 15 (2023) 10821.

[6] S. Saud, A. Yang, Z. Jiang, D. Ning, S. Fahad, New insights in to the environmental behavior and ecological toxicity of microplastics, J. Hazard. Mater. Adv. 10 (2023) 100298, https://doi.org/10.1016/j.hazadv.2023.100298.

[7] S.M. Praveena, Exploring public awareness, influencing factors and policy implications towards microplastic pollution: Perspectives from Malaysia, Mar. Policy 161 (2024) 106042, https://doi.org/10.1016/j.marpol.2024.106042.

[8] N. Badola, A. Bahuguna, Y. Sasson, J.S. Chauhan, Microplastics removal strategies: A step toward finding the solution, Front. Environ. Sci. Eng. 16 (1) (2022) 7.

[9] Y. Zhang, H. Jiang, K. Bian, H. Wang, C. Wang, A critical review of control and removal strategies for microplastics from aquatic environments, J. Environ. Chem. Eng. 9 (2021) 105463, https://doi.org/10.1016/j.jece.2021.105463.

[10] K. Elsaid, A.G. Olabi, A. Abdel-Wahab, A. Elkamel, A.H. Alami, A. Inayat, K.-J. Chae, M.A. Abdelkareem, Membrane processes for environmental remediation of nanomaterials: potentials and challenges, Sci. Total Environ. 879 (2023) 162569, https://doi.org/10.1016/j.scitotenv.2023.162569.

[11] C. Akarsu, H. Kumbur, A.E. Kideys, Removal of microplastics from wastewater through electrocoagulation-electroflotation and membrane filtration processes, Water Sci. Technol. 84 (7) (2021) 1648, https://doi.org/10.2166/wst.2021.356.

[12] C. Hachemi, M. Enfrin, A.O. Rashed, V. Jegatheesan, P.D. Hodgson, D.L. Callahan, J. Lee, L.F. Dumée, The impact of PET microplastic fibres on PVDF ultrafiltration performance – A short-term assessment of MP fouling in simple and complex matrices, Chemosphere 310 (2023) 136891, https://doi.org/10.1016/j.chemosphere.2022.136891.

[13] H. Kook, C. Park, Engineered approaches to facile identification of tiny microplastics in polymeric and ceramic membrane filtrations for wastewater treatment, Membranes 12 (2022) 565.

[14] S.A. Markazi, M. Karimi, B. Yousefi, M. Sadati, H. Khoramshahi, S. Khoee, M. R. Karimi, Experimental and modeling study on the simultaneous fouling behavior of micro/nanoplastics and bovine serum albumin in ultrafiltration membrane separation, J. Environ. Chem. Eng. 11 (2023) 109354, https://doi.org/10.1016/j.jece.2023.109354.

[15] K. Juraij, S.P. Ammed, C. Chingakham, B. Ramasubramanian, S. Ramakrishna, S. Vasudevan, A. Sujith, Electrospun polyurethane nanofiber membranes for microplastic and nanoplastic separation, ACS Appl. Nano Mater. 6 (6) (2023) 4636–4650, https://doi.org/10.1021/acsanm.3c00112.

[16] A.R.P. Pizzichetti, C. Pablos, C. Álvarez-Fernández, K. Reynolds, S. Stanley, J. Marugán, Evaluation of membranes performance for microplastic removal in a simple and low-cost filtration system, Case Stud. Chem. Environ. Eng. 3 (2021) 100075, https://doi.org/10.1016/j.cscee.2020.100075.

[17] S. Dong, M. Zhou, X. Su, J. Xia, L. Wang, H. Wu, E.B. Suakollie, D. Wang, Transport and retention patterns of fragmental microplastics in saturated and unsaturated porous media : A real-time pore-scale visualization, Water Res. 214 (2022) 118195, https://doi.org/10.1016/j.watres.2022.118195.

[18] S.H. Na, M.J. Kim, J.T. Kim, S. Jeong, S. Lee, J. Chung, E.J. Kim, Microplastic removal in conventional drinking water treatment processes: Performance, mechanism, and potential risk, Water Res. 202 (2021) 117417, https://doi.org/10.1016/j.watres.2021.117417.

[19] M. Umar, C. Singdahl-Larsen, S.B. Ranneklev, Microplastics removal from a plastic recycling industrial wastewater using sand filtration, Water (Switzerland) 15 (2023) 896, https://doi.org/10.3390/w15050896.

[20] M. Shen, T. Hu, W. Huang, B. Song, G. Zeng, Y. Zhang, Removal of microplastics from wastewater with aluminosilicate filter media and their surfactant-modified products: Performance, mechanism and utilization, Chem. Eng. J. 421 (2021) 129918, https://doi.org/10.1016/j.cej.2021.129918.

[21] J. Gonzalez-Camejo, A. Morales, J. Pena-Lamas, C. Lafita, S. Enguídanos, A. Seco, N. Martí, Feasibility of rapid gravity filtration and membrane ultrafiltration for the removal of microplastics and microlitter in sewage and wastewater from plastic industry, J. Water Process Eng. 51 (2023) 103452, https://doi.org/10.1016/j.jwpe.2022.103452.

[22] G. Pulido-Reyes, L. Magherini, C. Bianco, R. Sethi, U. von Gunten, R. Kaegi, D. M. Mitrano, Nanoplastics removal during drinking water treatment: Laboratory- and pilot-scale experiments and modeling, J. Hazard. Mater. 436 (2022) 129011, https://doi.org/10.1016/j.jhazmat.2022.129011.

[23] M. Ahmad, N.M.A. Lubis, M. Usama, J. Ahmad, M.I. Al-Wabel, H.A. Al-Swadi, M. I. Rafique, A.S.F. Al-Farraj, Scavenging microplastics and heavy metals from water using jujube waste-derived biochar in fixed-bed column trials, Environ. Pollut. 335 (2023) 122319, https://doi.org/10.1016/j.envpol.2023.122319.

[24] L. Hsieh, L. He, M. Zhang, W. Lv, K. Yang, M. Tong, Addition of biochar as thin preamble layer into sand filtration columns could improve the microplastics removal from water, Water Res. 221 (2022) 118783, https://doi.org/10.1016/j.watres.2022.118783.

[25] X. Li, Y. Zhang, H. Xu, Y. Sun, B. Gao, J. Wu, Granular limestone amended sand filters for enhanced removal of nanoplastics from water : Performance and mechanisms, Water Res. 229 (2023) 119443, https://doi.org/10.1016/j.watres.2022.119443.

[26] G. Ji, Y. Xing, T. You, Biochar as adsorbents for environmental microplastics and nanoplastics removal, J. Environ. Chem. Eng. 12 (2024) 113377, https://doi.org/10.1016/j.jece.2024.113377.

[27] J. Wu, C. Yang, H. Zhao, J. Shi, Z. Liu, C. Li, F. Song, Efficient removal of microplastics from aqueous solution by a novel magnetic biochar: performance, mechanism, and reusability, Environ. Sci. Pollut. Res. 30 (2023) 26914–26928, https://doi.org/10.1007/s11356-022-24130-1.

[28] N. Parashar, S. Hait, Cetyl trimethyl ammonium bromide-modified magnetic biochar-integrated sand filter for microplastics removal from secondary-treated sewage effluents: Performance evaluation and mechanistic insights, J. Water Process Eng. 59 (2024) 105035, https://doi.org/10.1016/j.jwpe.2024.105035.

[29] V. Siipola, S. Pflugmacher, H. Romar, L. Wendling, P. Koukkari, Low-cost biochar adsorbents for water purification including microplastics removal, Appl. Sci. 10 (2020) 788.

[30] A. Subair, P. Krishnamoorthy Lakshmi, S. Chellappan, C. Chinghakham, Removal of polystyrene microplastics using biochar-based continuous flow fixed-bed column, Environ. Sci. Pollut. Res. 31 (2024) 13753–13765, https://doi.org/10.1007/s11356-024-32088-5.

[31] Z. Wang, M. Sedighi, A. Lea-Langton, Filtration of microplastic spheres by biochar: removal efficiency and immobilisation mechanisms, Water Res. 184 (2020) 116165, https://doi.org/10.1016/j.watres.2020.116165.

[32] S. Dong, J. Xia, L. Sheng, W. Wang, H. Liu, B. Gao, Transport characteristics of fragmental polyethylene glycol terephthalate (PET) microplastics in porous media under various chemical conditions, Chemosphere 276 (2021) 130214, https://doi.org/10.1016/j.chemosphere.2021.130214.

[33] H.A. Murad, M. Ahmad, J. Bundschuh, Y. Hashimoto, M. Zhang, B. Sarkar, Y.S. Ok, A remediation approach to chromium-contaminated water and soil using engineered biochar derived from peanut shell, Environ. Res. 204 (2022) 112125, https://doi.org/10.1016/j.envres.2021.112125.

[34] Z. Hua, Y. Pan, Q. Hong, Adsorption of Congo red dye in water by orange peel biochar modified with CTAB, RSC Adv. 13 (2023) 12502, https://doi.org/10.1039/d3ra01444d.

[35] C. Kosaiyakanon, S. Kungsanant, Adsorption of reactive dyes from wastewater using cationic surfactant-modified coffee husk biochar, Environ. Nat. Resources J. 18 (1) (2020) 21–32, https://doi.org/10.32526/ennrj.18.1.2020.03.

[36] G. Li, H. Li, X. Mi, W. Zhao, Enhanced adsorption of Orange II on bagasse-derived biochar by direct addition of CTAB, Korean J. Chem. Eng. 36 (8) (2019) 1274–1280, https://doi.org/10.1007/s11814-019-0304-0.

[37] H. Wang, S. Wang, Y. Gao, Cetyl trimethyl ammonium bromide modified magnetic biochar from pine nut shells for efficient removal of acid chrome blue K, Bioresour. Technol. 312 (2020) 123564, https://doi.org/10.1016/j.biortech.2020.123564.

[38] L. Mathurasa, S. Damrongsiri, Low cost and easy rice husk modification to efficiently enhance ammonium and nitrate adsorption, Int. J. Recycling Org. Waste Agri. 7 (2018) 143–151, https://doi.org/10.1007/s40093-018-0200-3.

[39] T. Mehmood, A.U. Khan, K.P. Raj Dandamudi, S. Deng, M.H. Helal, H.M. Ali, Z. Ahmad, Oil tea shell synthesized biochar adsorptive utilization for the nitrate removal from aqueous media, Chemosphere 307 (2022) 136045, https://doi.org/10.1016/j.chemosphere.2022.136045.

[40] Y. Shi, J. Du, T. Zhao, B. Feng, H. Bian, S. Shan, J. Meng, P. Christie, M.H. Wong, J. Zhang, Removal of nanoplastics from aqueous solution by aggregation using reusable magnetic biochar modified with cetyltrimethylammonium bromide, Environ. Pollut. 318 (2023) 120897, https://doi.org/10.1016/j.envpol.2022.120897.

[41] Y. Xing, B. Zhang, Q. Niu, G. Ji, Enhanced adsorption of polystyrene nanoplastics by cetyltrimethylammonium bromide surface-modified magnetic rice straw biochar: efficient performance and adsorption mechanisms, Sep. Purif. Technol. 344 (2024) 127264, https://doi.org/10.1016/j.seppur.2024.127264.

[42] A. Misra, C. Zambrzycki, G. Kloker, A. Kotyrba, M.H. Anjass, I.F. Castillo, S. G. Mitchell, R. Güttel, C. Streb, Water purification water purification and microplastics removal using magnetic polyoxometalate-supported ionic liquid phases (magPOM-SILPs), Angew. Chemie – Int. Ed. 59 (2020) 1601–1605, https://doi.org/10.1002/anie.201912111.

[43] M.A. Hanif, N. Ibrahim, F.A. Dahalan, U.F. Md Ali, M. Hasan, A.W. Azhari, A. Abdul Jalil, Microplastics in facial cleanser: extraction, identification, potential toxicity, and continuous-flow removal using agricultural waste–based biochar, Environ. Sci. Pollut. Res. 30 (2023) 60106–60120, https://doi.org/10.1007/s11356-023-26741-8.

[44] Y.-J. Chen, Y. Chen, C. Miao, Y.-R. Wang, G.-K. Gao, R.-X. Yang, H.-J. Zhu, J.-H. Wang, S.-L. Li, Y.-Q. Lan, Metal-organic framework based foams for efficient microplastic removal, J. Mater. Chem. A 8 (2020) 14644–14652, https://doi.org/10.1039/D0TA04891G.

[45] F. Yuan, L. Yue, H. Zhao, H. Wu, Study on the adsorption of polystyrene microplastics by three-dimensional reduced graphene oxide, Water Sci. Technol. 81 (10) (2020) 2163–2175, https://doi.org/10.2166/wst.2020.269.

[46] Kumarasiri, A., Amarasinghe, D. A. S., & Attygalle, D. (2020). Surface Wettability Analysis of Nichrome Alloy Based on the Measurements of Sessile Droplet Contact Angles. MERCon 2020 - 6th International Multidisciplinary Moratuwa Engineering Research Conference, Proceedings, 160–164. doi: 10.1109/MERCon50084.2020.9185360.

[47] O. Rius-Ayra, A. Biserova-Tahchieva, N. LLorca-Isern, Surface-functionalised materials for microplastic removal, Mar. Pollut. Bull. 167 (2021) 112335, https://doi.org/10.1016/j.marpolbul.2021.112335.

[48] J. Wu, Y. Zhang, Y. Tang, Fragmentation of microplastics in the drinking water treatment process - A case study in Yangtze River region, China. Sci. Total Environ. 806 (2022) 150545, https://doi.org/10.1016/j.scitotenv.2021.150545.

[49] D.W. Skaf, V.L. Punzi, J.T. Rolle, K.A. Kleinberg, Removal of micron-sized microplastic particles from simulated drinking water via alum coagulation, Chem. Eng. J. 386 (2020) 123807, https://doi.org/10.1016/j.cej.2019.123807.

[50] D. Elkhatib, V. Oyanedel-Craver, E. Carissimi, Electrocoagulation applied for the removal of microplastics from wastewater treatment facilities, Sep. Purif. Technol. 276 (2021) 118877, https://doi.org/10.1016/j.seppur.2021.118877.

[51] S. Mondal, S.K. Majumder, Cationic surfactant-aided surface modification of the activated carbon-based materials for the enhancement of phenol adsorption-capacity determined by ultraviolet-visible spectroscopy, J. Dispers. Sci. Technol. 43 (13) (2021) 1–15, https://doi.org/10.1080/01932691.2021.1884089.

[52] A.A. Ajeng, R. Abdullah, A. Junia, B.F. Lau, T.C. Ling, S. Ismail, Evaluation of palm kernel shell biochar for the adsorption of Bacillus cereus Evaluation of palm kernel shell biochar for the adsorption of Bacillus cereus, Phys. Scr. 96 (2021) 105004.

[53] W. Dechapanya, A. Khamwichit, Biosorption of aqueous Pb(II) by H_3PO_4-activated biochar prepared from palm kernel shells (PKS), Heliyon 9 (2023) e17250, https://doi.org/10.1016/j.heliyon.2023.e17250.

[54] K.K. Katibi, K.F. Yunos, H. Che Man, A.Z. Aris, M.Z. Mohd Nor, R.S. Azis, An insight into a sustainable removal of bisphenol a from aqueous solution by novel palm kernel shell magnetically induced biochar: synthesis, characterization, kinetic, and thermodynamic studies, Polymers 13 (2021) 3781.

[55] S. Khawkomol, R. Neamchan, T. Thongsamer, S. Vinitnantharat, B. Panpradit, P. Sohsalam, D. Werner, W. Mrozik, Potential of biochar derived from agricultural residues for sustainable management, Sustainability (Switzerland) 13 (2021) 8147.

[56] T. Wang, Z. Meng, L. Sheng, Z. Liu, X. Cao, X. Wang, X. Sun, Insights into the mechanism of co-adsorption between tetracycline and nano-TiO_2 on coconut shell porous biochar in binary system, Adv. Powder Technol. 32 (2021) 4120–4129, https://doi.org/10.1016/j.apt.2021.09.014.

[57] S. Nagireddi, Effect of cetrimonium bromide (CTAB) surfactant on Pd(II) removal efficiency from electroless plating solutions, Mater. Today Proc. (2022), https://doi.org/10.1016/j.matpr.2022.06.259.

[58] C. Patra, R. Gupta, D. Bedadeep, S. Narayanasamy, Surface treated acid-activated carbon for adsorption of anionic azo dyes from single and binary adsorptive systems: A detail insight, Environ. Pollut. 266 (2020) 115102, https://doi.org/10.1016/j.envpol.2020.115102.

[59] D. Castilla-Caballero, A. Hernandez-Ramirez, S. Vazquez-Rodriguez, J. Colina-Marquez, F. Machuca-Martínez, J. Barraza-Burgos, A. Roa-Espinosa, A. Medina-Guerrero, S. Gunasekaran, Effect of pyrolysis, impregnation, and calcination conditions on the physicochemical properties of TiO2/Biochar composites intended for photocatalytic applications, J. Environ. Chem. Eng. 11 (2023) 110274, https://doi.org/10.1016/j.jece.2023.110274.

[60] Y. Zhu, Y. Cui, Y. Peng, R. Dai, H. Chen, Y. Wang, Preparation of CTAB intercalated bentonite for ultrafast adsorption of anionic dyes and mechanism study, Colloids Surf. A Physicochem. Eng. Asp. 658 (2023) 130705, https://doi.org/10.1016/j.colsurfa.2022.130705.

[61] X. Pan, Z. Gu, W. Chen, Q. Li, Preparation of biochar and biochar composites and their application in a Fenton-like process for wastewater decontamination: a review, Sci. Total Environ. 754 (2021) 142104, https://doi.org/10.1016/j.scitotenv.2020.142104.

[62] M.P. Schmidt, D.J. Ashworth, N. Celis, A.M. Ibekwe, Optimizing date palm leaf and pistachio shell biochar properties for antibiotic adsorption by varying pyrolysis temperature, Bioresour. Technol. Rep. 21 (2023) 101325, https://doi.org/10.1016/j.biteb.2022.101325.

[63] Z. Shi, P. Li, L. Liu, Interactions between CTAB and montmorillonite by atomic force microscopy and molecular dynamics simulation, Colloids Surf. A Physicochem. Eng. Asp. 657 (PB) (2023) 130656, https://doi.org/10.1016/j.colsurfa.2022.130656.

[64] F.M. Ivanic, G. Guggenberger, S.K. Woche, M. Hoppe, J.F. Carstens, Soil organic matter facilitates the transport of microplastic by reducing surface hydrophobicity, Colloids and Surf. a: Physicochem. Eng. Asp. 676 (2023) 132255, https://doi.org/10.1016/j.colsurfa.2023.132255.

[65] J. Gao, S. Pan, P. Li, L. Wang, R. Hou, W.M. Wu, J. Luo, D. Hou, Vertical migration of microplastics in porous media: Multiple controlling factors under wet-dry cycling, J. Hazard. Mater. 419 (2021) 126413, https://doi.org/10.1016/j.jhazmat.2021.126413.

[66] Z.A. Ganie, N. Khandelwal, E. Tiwari, N. Singh, K. Darbha, Biochar-facilitated remediation of nanoplastic contaminated water : Effect of pyrolysis temperature induced surface modifications, J. Hazard. Mater. 417 (2021) 126096, https://doi.org/10.1016/j.jhazmat.2021.126096.

[67] P.L. Yen, C.-H. Hsu, M.-L. Huang, V.-H.-C. Liao, Removal of nano-sized polystyrene plastic from aqueous solutions using untreated coffee grounds, Chemosphere 286 (2022) 131863, https://doi.org/10.1016/j.chemosphere.2021.131863.

[68] F. Wang, W. Sha, X. Wang, Y. Shang, L. Hou, Y. Li, Adsorption of 17 α -ethinyl estradiol and bisphenol a to graphene-based materials: effects of configuration of adsorbates and the presence of cationic surfactant, Adsorpt. Sci. Technol. 2021 (2021) 9970268, https://doi.org/10.1155/2021/9970268.

[69] S. Kalam, S.A. Abu-khamsin, M.S. Kamal, S. Patil, Surfactant adsorption isotherms: a review, ACS Omega 6 (2021) 32342–32348, https://doi.org/10.1021/acsomega.1c04661.

[70] H.J. Shupe, K.M. Boenisch, B.J. Harper, S.M. Brander, S.L. Harper, Effect of nanoplastic type and surface chemistry on particle agglomeration over a salinity gradient, Environ. Toxicol. Chem. 40 (7) (2021) 1822–1828, https://doi.org/10.1002/etc.5030.

[71] M. Enfrin, J. Lee, P. Le-Clech, L.F. Dumée, Kinetic and mechanistic aspects of ultrafiltration membrane fouling by nano- and microplastics, J. Membr. Sci. 601 (2020) 117890, https://doi.org/10.1016/j.memsci.2020.117890.

[72] L. Ramirez Arenas, S. Ramseier Gentile, S. Zimmermann, S. Stoll, Fate and removal efficiency of polystyrene nanoplastics in a pilot drinking water treatment plant, Sci. Total Environ. 813 (2022) 152623, https://doi.org/10.1016/j.scitotenv.2021.152623.

[73] H.J. Kwon, H. Hidayaturrahman, S.G. Peera, T.G. Lee, Elimination of microplastics at different stages in wastewater treatment plants, Water (Switzerland) 14 (2022) 2404, https://doi.org/10.3390/w14152404.

[74] G. Rullander, C. Lorenz, R.B. Herbert, A.M. Strömvall, J. Vollertsen, S.S. Dalahmeh, How effective is the retention of microplastics in horizontal flow sand filters treating stormwater? J. Environ. Manage. 344 (2023) 118690 https://doi.org/10.1016/j.jenvman.2023.118690.

[75] F.C. Tumwet, R. Serbe, T. Kleint, T. Scheytt, Effect of fragmentation on the transport of polyvinyl chloride and low-density polyethylene in saturated quartz sand, Sci. Total Environ. 836 (2022) 155657, https://doi.org/10.1016/j.scitotenv.2022.155657.

[76] K. Waldschläger, H. Schüttrumpf, Infiltration behavior of microplastic particles with different densities, sizes, and shapes-from glass spheres to natural sediments, Environ. Sci. Tech. 54 (15) (2020) 9366–9373, https://doi.org/10.1021/acs.est.0c01722.

[77] S. Acarer, Microplastics in wastewater treatment plants: Sources, properties, removal efficiency, removal mechanisms, and interactions with pollutants, Water Sci. Technol. 87 (3) (2023) 685, https://doi.org/10.2166/wst.2023.022.

[78] X. Zhang, Y. Chen, X. Li, Y. Zhang, W. Gao, J. Jiang, A. Mo, D. He, Size/shape-dependent migration of microplastics in agricultural soil under simulative and natural rainfall, Sci. Total Environ. 815 (2022) 152507, https://doi.org/10.1016/j.scitotenv.2021.152507.

[79] V.P. Ranjan, A. Joseph, H.B. Sharma, S. Goel, Preliminary investigation on effects of size, polymer type, and surface behaviour on the vertical mobility of microplastics in a porous media, Sci. Total Environ. 864 (2023) 161148, https://doi.org/10.1016/j.scitotenv.2022.161148.

[80] N.N.A. Mohd Napi, N. Ibrahim, M.A. Hanif, M. Hasan, F.A. Dahalan, A. Syafiuddin, R. Boopathy, Column-based removal of high concentration microplastics in synthetic wastewater using granular activated carbon, Bioengineered 14 (1) (2023) 2276391, https://doi.org/10.1080/21655979.2023.2276391.

[81] M. Tong, T. Li, M. Li, L. He, Z. Ma, Cotransport and deposition of biochar with different sized-plastic particles in saturated porous media, Sci. Total Environ. 713 (2020) 136387, https://doi.org/10.1016/j.scitotenv.2019.136387.

[82] K.N. Palansooriya, P.A. Withana, Y. Jeong, M.K. Sang, Y. Cho, G. Hwang, S. X. Chang, Y.S. Ok, Contrasting effects of food waste and its biochar on soil properties and lettuce growth in a microplastic-contaminated soil, Appl. Biol. Chem. 67 (2024) 3, https://doi.org/10.1186/s13765-023-00851-w.

[83] L. Zhang, Q. Zhang, Y. Wang, X. Cui, Y. Liu, R. Ruan, X. Wu, L. Cao, L. Zhao, H. Zheng, Preparation and application of metal-modified biochar in the purification of micro-polystyrene polluted aqueous environment, J. Environ. Manage. 347 (2023) 119158, https://doi.org/10.1016/j.jenvman.2023.119158.

[84] A. Aslam, S.J. Khan, H.M.A. Shahzad, Anaerobic membrane bioreactors (AnMBRs) for municipal wastewater treatment- potential benefits, constraints, and future perspectives: An updated review, Sci. Total Environ. 802 (2022) 149612, https://doi.org/10.1016/j.scitotenv.2021.149612.

[85] W.H. Abuwatfa, D. Al-Muqbel, A. Al-Othman, N. Halalsheh, M. Tawalbeh, Insights into the removal of microplastics from water using biochar in the era of COVID-19: A mini review, Case Stud. Chem. Environ. Eng. 4 (2021) 100151, https://doi.org/10.1016/j.cscee.2021.100151.